THE JOURNAL OF PHYSICAL CHEMISTRY B

Article

pubs.acs.org/JPCB

Role of Hydrophobic Hydration in Protein Stability: A 3D Water-Explicit Protein Model Exhibiting Cold and Heat Denaturation

Silvina Matysiak,*[,†] Pablo G. Debenedetti,[‡] and Peter J. Rossky[¶]

[†]Fischell Department of Bioengineering, University of Maryland, College Park, Maryland 20742, United States

[‡]Department of Chemical and Biological Engineering, Princeton University, Princeton, New Jersey 08544, United States

[¶]Institute for Computational Engineering and Sciences and Department of Chemistry and Biochemistry, University of Texas at Austin, Austin, Texas 78712, United States

ABSTRACT: We investigate the microscopic mechanism of cold and heat denaturation using a 3D lattice model of a hydrated protein in which water is represented explicitly. The water model, which incorporates directional bonding and tetrahedral geometry, captures many aspects of water thermodynamics and properly describes hydrophobic hydration around apolar solutes because the hydrogen bonding rules in the model were gleaned from off-lattice atomistic simulations of water around representative protein structures. By incorporating local chain stiffness in the protein model, a homopolymer can fold into a β-hairpin. It is shown that the homopolymer can be folded by either attractive interactions between the monomers or as a direct consequence of the entropic cost of forming interfacial hydrogen bonds in the solvent. However, cold denaturation is not observed if the collapse transition is induced by intramolecular attractions. We further find that it is the changes in hydrophobic hydration with decreasing temperature that drive cold unfolding and that the overall process is enthalpically driven, whereas heat denaturation is entropically driven.

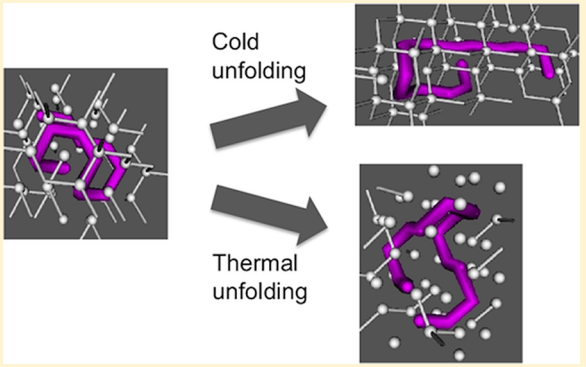

INTRODUCTION

Under physiological conditions, proteins adopt a unique three-dimensional, biologically active structure. The high cooperativity of the folding process simplifies the analysis of protein stability, allowing many single-domain proteins to be described in terms of a two-state equilibrium between a native and a denatured state. While ordered molecular systems are usually increasingly more stable at low temperatures, where thermal fluctuations are modest, native protein folds tend to be stable over a limited intermediate range of temperatures and possess a temperature of maximum stability within this range.[1,2] As a consequence, the native conformation of a protein can be disrupted by either heating or cooling, in addition to pressure and chemical denaturation. The stability of the native state is the result of several contributions, including hydrogen bonds and electrostatic and hydrophobic interactions.[3] Hydrogen bonding is crucial for the formation of secondary structures, while electrostatic and hydrophobic interactions are necessary for stabilizing the tertiary structure of proteins. The subtle change in the relative strength of these interactions lies at the heart of protein denaturation.

Recent experimental work indicates that there is a difference in the denatured states obtained by cold and heat denaturation; cold-denatured proteins are more compact but exhibit solvent penetration, while heat-unfolded proteins are more extended.[4,5] Heat denaturation is primarily due to the increase of conformational entropy as the polypeptide chain unfolds, leading to a largely extended conformation, a typical polymer behavior. On the other hand, cold denaturation is believed to be a milder form of structural loss, leading to a partial unfolding of the protein.[6] Cold denaturation is thought to proceed largely as a result of changes in the nature of the interaction between water and nonpolar groups. As the temperature is decreased, the free-energy penalty of the entropically unfavorable interaction between water and the hydrophobe becomes smaller, leading to an increased tendency for nonpolar group hydration.[2,7] The experimentally observed loss of tertiary interactions in cold denaturation[4,5,8−14] then reflects a weakening of hydrophobic associations. Thus, obtaining a microscopic picture of the cold denaturation phenomenon would facilitate the understanding of the forces responsible for the structure of folded proteins and the complex role played by the hydrophobic effect.

Atomistically detailed simulations of proteins have provided substantial insight into the mechanism of protein denaturation and the formation of native state structure, such as the villin headpiece,[15] Trp-cage miniprotein,[16] a β-hairpin,[17] and BBA5.[18] Other studies have examined the role of water in protein folding for larger systems such as protein SH3[19] and BphC enzyme.[20] In general, explicit solvent molecular dynamics

Received: April 23, 2012
Revised: June 20, 2012
Published: June 23, 2012

dx.doi.org/10.1021/jp3039175 | J. Phys. Chem. B 2012, 116, 8095−8104

are commonly used to study short-time dynamics due to the limitation resulting from the long times required to simulate large-scale conformational changes. A study of protein stability using straightforward molecular dynamics simulations with explicit solvation is practically impossible due to slow kinetics, resulting in insufficient conformational sampling at low temperatures and high pressures.[21] A productive approach to access the cold-denatured region in explicit simulations of proteins uses replica-exchange simulations at high pressure[22] to extrapolate the pressure−temperature stability diagram using Hawley theory[16,23] or performs umbrella sampling simulations,[24] but even then, only quite small peptide sequences have been successfully studied.

Simple protein models where residues are represented by one (or a few) bead(s) have been very valuable in advancing our understanding of the folding process, particularly when used in combination with experiments.[25,26] The ability of such models to reproduce the essential features of folding dynamics suggests that each single atomic degree of freedom is not by itself particularly relevant to the generic behavior of folding and supports a statistical mechanical approach to characterize folding transitions. A key element in most minimalist models of proteins that capture secondary structure elements is that they renormalize the role of water by using implicit solvent models with effective interactions for the short-ranged interaction energy parameters among residues.[27−29] However, an important drawback of not modeling the solvent explicitly is the fact that the effect of changing the thermodynamic conditions cannot be studied in a predictive way, and the critical manner in which water participates in protein folding is not accessible to investigation; such effects are buried in the parametrization of the effective interactions. As a collorary, another disadvantage of current minimalist models that capture secondary structure elements is that in those models, the ground state is also the protein's native state, which precludes the existence of a denatured state that can be more stable than the native state at lower temperatures without a change in model parameters with temperature. Thus, an implicit description of the solvent is unlikely to account for both cold and heat denaturation unless the model parameters are fitted to thermodynamic properties (e.g., temperature-dependent energetics). In this regard, Whitten and co-workers have developed a protein model that seeks to differentiate the cooperative substructure of proteins based on fundamental thermodynamic parameters that are empirically derived.[30] A structurally resolved view of the cold denaturation process was obtained using the model of Whitten in which cold-unfolded states correspond to partially folded states. However, because the model parameters are linked to thermodynamic properties, a mechanistic description of the cold denaturation process cannot be obtained with such models. When the solvent is described explicitly, both heat and cold denaturation can be recovered naturally from first principles.[31−34]

Cold denaturation has been studied using two-dimensional (2D) conformational spaces and minimalist explicit solvent models that take hydrophobicity into account. One class of models uses a bimodal description of water, distinguishing between bulk and solvation shell waters in their energy and entropy.[35] Another class of models couple the compactness of the protein to the bulk water structure, linking a local property of the protein to an average bulk property of water.[33] Recently, some of the present authors have shown that an explicit treatment of hydrophobic hydration is sufficient to produce cold, pressure, and thermal denaturation in a 2D lattice model of a hydrophobic homoprotein in explicit water.[31] However, due to the 2D geometry, water molecules in the hydrophobic protein hydration shell must, in every case, lose at least one hydrogen bond because they cannot form one with the homoprotein and, in 2D in contrast to 3D, the linear topology of the polymer blocks the maintenance of a continuous hydrogen bond network at its boundary. Atomistic simulations have shown that each water molecule in the hydration shell around hydrophobic residues is strongly inclined to retain its hydrogen bonds, leading inevitably to a significant orientational constraint for water molecules at the surface of nonpolar residues.[36−38] A 3D water-explicit protein model would allow, in principle, to capture this effect, allowing hydrophobic hydration water molecules to statistically select orientations in a way that avoids sacrificing its hydrogen bonds. Furthermore, a 3D description would also allow for the modeling of the characteristic secondary structural elements of proteins, which is not possible in a 2D model. This would open the door to investigating the relationship between sequence, protein fold, and stability.

We present here a 3D lattice model of a globular protein in explicit water, developed from first principles, that exhibits cold and thermal denaturation and examine the microscopic physical mechanism behind cold and heat denaturation. This model is not intended for making quantitative predictions but rather as a tool for exploring mechanisms and, particularly, the role of hydrophobic hydration in the cold denaturation process. The protein model is inspired by the tetrahedral lattice model of Kolinski et al. that allows the formation of secondary structural elements including α-helices, β-sheets, and β-hairpins.[39,40] The approach pursued in this paper will enrich this important class of models by including water explicitly; the hydrophobic interaction of residues arises not due to explicit attractive interactions between hydrophobic monomers in the model but by explicitly taking into account the manner in which the hydrophobic residues interact with water.

The outline of this paper is as follows. We begin with a description of the microscopic model and the origins of the solvation model from first principles. We also discuss the methodology used to compute the model's density of states and properties. We then examine the temperature dependence of the properties of a flexible homopolymer for different parametrizations and discuss the driving forces behind the collapse and denaturation transitions. We also study the effect of including local conformational stiffness into the protein model and show that a homoprotein can be folded into a β-hairpin. Finally, we present the main conclusions, as well as possible extensions of the model and of these studies.

MODEL DESCRIPTION

The protein aqueous solution is defined on a body-centered cubic (BCC) lattice, which contains single-site molecules as the solvent and a self-avoiding chain of connected sites representing the homopolymer. The homopolymer lies on one of the tetrahedral sublattices present in the BCC lattice to satisfy the tetrahedral angle observed between C_α atoms in protein structures. Each site in the lattice can be either empty or filled by a water molecule or a protein monomer, as shown in Figure 1.

The protein Hamiltonian is inspired by the previous work of Skolnick and co-workers[40,41] on a minimalist 3D model that captures key aspects of protein folding, including cooperative,

dx.doi.org/10.1021/jp3039175 | J. Phys. Chem. B 2012, 116, 8095−8104

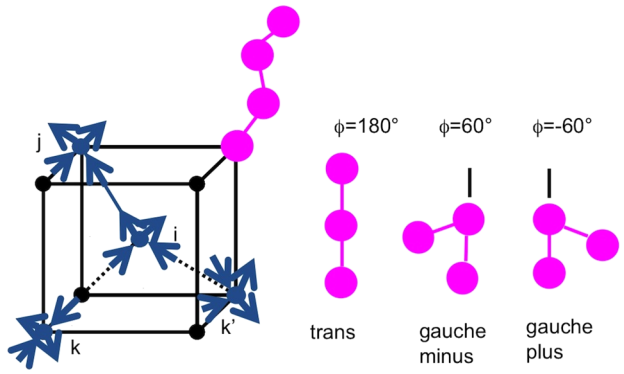

Figure 1. Illustration of the relative positions of interacting water molecules; dotted lines indicate nonbonding pairs, and bold full lines indicate hydrogen-bonded pairs. Molecules *i* and *j* are in a correct configuration for bonding because a donor arm of molecule *i* points toward an acceptor arm of molecule *j*. Molecules *i* and *k* are nonbonded because a donor arm of molecule *i* points toward a donor arm of molecule *k*. Molecules *i* and *k*′ are nonbonded because molecule *k*′ does not have an arm pointing toward molecule *i*. The black sites in the BCC lattice are empty, whereas the pink ones correspond to monomers. A schematic representation of the three possible conformational states available to three successive bonded sites along the chain is illustrated on the right portion of the figure.

"all-or-nothing" folding into stable and nondegenerate compact states with distinct structural motifs. The protein is modeled as a self-avoiding walk in the underlying tetrahedral lattice present in the total BCC lattice with covalently attached monomers occupying nearest-neighbor (denoted hereafter by "nn") sites on the lattice. Three discrete conformations of every three-bond sequence are allowed, one planar trans (t) and two out-of-plane gauche minus (g^-) and gauche plus (g^+) conformations, as shown in Figure 1. Thus, each bond in the protein is represented as a vector of the form $[\pm1,\pm1,\pm1]$ with a total bond length of $\sqrt{3}$. The "protein" that we consider here is a 14-monomer homopolymer, and each monomer is nonpolar.

To study the folding of β-hairpin polypeptides, the local conformational stiffness needs to be introduced by a priori energetic preference (ε_g) for the t conformation over either of the two g states. The soft attractive part of the short-range intrinsic monomer–monomer interaction is taken to be of the form of a square-well potential of depth ε_{mm} whose width extends only to the nonbonded nn sites on the lattice. Thus, the homopolymer configurational energy of a given conformation of the chain is given by the expression

$$H_p = \sum_{i=2}^{n-2} (1 - f_{t,i})\varepsilon_g + \frac{1}{2}\sum_{i=1}^{n}\sum_{|j-i|>1}^{n} \delta(r_{ij} - l)\varepsilon_{mm} \quad (1)$$

where $f_{t,i} = 1$ for the t state of the rotational degree of freedom associated with the *i*th bond ($f_{t,i} = 0$ for a g state or for end bonds), $r_{i,j}$ is the distance between the beads under consideration, and l is the lattice spacing equal to the length of a bond. The hard-core part of local interactions between beads of the model chain is introduced by a priori exclusion of multiple occupancy of lattice sites. α-Helices can also be studied with this model by incorporating a monomer–monomer interaction that favors the formation of helical contacts.

The water model is inspired by the Roberts–Debenedetti model, which captures key aspects of the distinctive thermodynamics of liquid water, such as the density anomaly and the possibility of a low-temperature liquid–liquid transition.[42,43] Each water molecule has four bonding arms in a tetrahedral arrangement, representing two proton-donor arms and two proton-acceptor arms. The number of distinguishable orientations available to a given molecule is q. Bonded states constitute a small fraction of the number of possible mutual orientations. Molecules are not restricted to be oriented such that their arms point only toward nn sites (as shown in Figure 1 by the water molecule *k*′), and we account explicitly for all possible orientations, including geometric restrictions due to the rigidity of the bonding arms.

For bond formation to occur, two nn molecules must have a donor–acceptor pair of arms properly oriented toward each other, as shown in Figure 1 by the *ij* water pair. Due to the lattice geometry, hydrogen bonds could in principle be formed between water molecules that lie on opposite sides of a polymer surface. To avoid this artifact, the formation of hydrogen bonds is not allowed whenever the pair of water molecules is proximal to more than three pairs of monomers that are also nearest neighbors to each other, as shown in Figure 2 by the black hydrogen bonds.

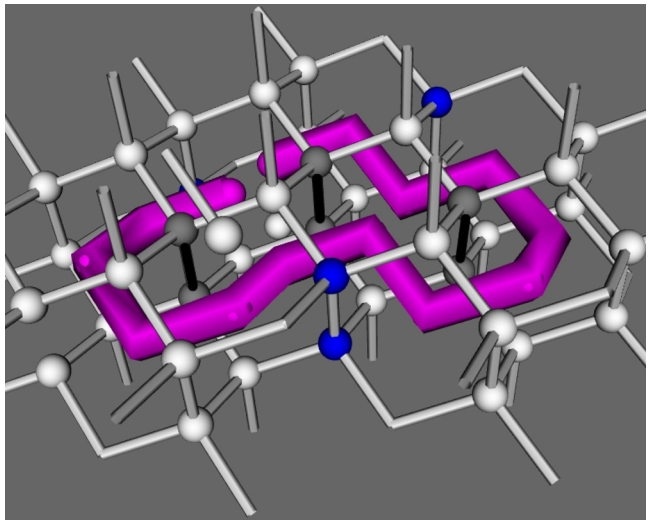

Figure 2. A conformation of the homopolymer with its hydration shell. The gray water molecules have three nearest-neighbor monomers, the blue ones have two, and the white ones have one nearest-neighbor monomer. Hydrogen bonds are represented as line segments joining participating water molecules. The black hydrogen bonds are proximal to more than three pairs of monomers that are nearest neighbors to each other. These hydrogen bonds are not allowed to form in the model because the water molecules forming these hydrogen bonds lie on opposite sides of a polymer surface.

In our previous work, we have found that in liquid water, there is a strong correlation between the interaction energy among nn water molecules and the local packing of water molecules around the pair, and we have quantitatively analyzed both intermolecular energy distributions and these correlations.[38] To account for this environmental dependence, the interaction energy of nn water molecules is defined to be a function of the local environment. The energy for hydrogen bonds (ε_{hb}) and for non-hydrogen-bonded pairs ($\varepsilon_{no\text{-}hb}$) depends on the total number of water molecules around the interacting pair (nn_{pair}) and is extracted from Figure 2 in ref 38. The total Hamiltonian for water–water interactions is given by

dx.doi.org/10.1021/jp3039175 | J. Phys. Chem. B 2012, 116, 8095–8104

$$H_{w-w} = \sum_{\langle i,j \rangle} nw_j nw_i \delta(r_{ij} - l)[\delta_{\sigma_i\sigma_j}\varepsilon_{hb}(nn_{pair_{ij}}) + (1 - \delta_{\sigma_i\sigma_j})\varepsilon_{no\text{-}hb}(nn_{pair_{ij}})] \quad (2)$$

where nw_i is an occupation variable for site i; $nw_i = 0$ if the site is empty or occupied by a protein monomer, and $nw_i = 1$ if it is occupied by a water molecule; $r_{i,j}$ is the distance between two water molecules, and l is the lattice spacing. The orientation of a water molecule i is not explicitly represented on the lattice but is described by the variable σ_i. Each water molecule has q possible orientations; thus, σ_i can take on values between 1 and q. The symbol $\delta_{\sigma i \sigma j}$ is a Kronecker delta; it is given the value 1 if a donor and an acceptor arm are pointing toward each other and is 0 otherwise.

We extend the hydrogen bonding interaction of the pure water model by differentiating water molecules into two classes, bulk and interfacial. Conceptually, these interfacial water molecules avoid orientations in which their hydrogen bonding arms point toward the hydrophobe, selecting from the more restrictive subset that is consistent with maintaining favorable water−water interactions in the first solvation shell. To adapt these ideas to our model, we follow earlier work[31] and allow a range of values of width λ for the mismatch of orientational parameters σ_i that will permit the formation of a hydrogen bond. A value of $\lambda = 0$ is equivalent to the original water model; that is, the orientations must match exactly. Here, we specify a separate width for bulk water (λ_B) and interfacial water (λ_h), with the latter being narrower ($\lambda_h < \lambda_B$). This reflects the more limited range of bonding geometries in the hydration shell. A bulk−bulk hydrogen bond is thus formed when the orientations of molecules i and j satisfy $|\sigma_i - \sigma_j| \leq \lambda_B$. For hydration layer water molecules, on the other hand, we require that the orientations match exactly, that is, $\sigma_i = \sigma_j$.

A water molecule is designated as interfacial when it is adjacent to one or more protein monomers. Along with the entropic cost of interfacial hydrogen bonds, there can be an enthalpic bonus. Because those hydrogen bonds that formed in more restricted orientational configurations around hydrophobic solutes less frequently sample the more distorted and weaker bonding structures present in bulk,[36,37] we consider the possibility that they have an enthalpic contribution (ε_{hb}^{+}) in addition to the base hydrogen bond strength ($\varepsilon_{hb}(nn_{pair_{ij}})$) (see Figure 2 in ref 38). The effect of including extra orientational restrictions (an entropic cost) or an extra enthalpic benefit for interfacial hydrogen bonds is considered in the Results section. Finally, the soft attractive part of the short-range water−monomer interaction is taken to be of the form of a square-well potential of depth ε_{wm} whose width extends only to nearest neighbors on the lattice. Thus, the total Hamiltonian of the system is as follows

$$H_{total} = H_{w-w} + H_p + \varepsilon_{wm}N_{wm} \quad (3)$$

where N_{wm} is the number of water−monomer contacts. The hard-core part of local interactions between beads of the model chain and water molecules is introduced by a priori exclusion of multiple occupancy of lattice sites.

To explore the balance between the entropic and enthalpic contributions to protein conformational stability, different types of parametrization of the interactions between polymer−polymer, polymer−water, and hydration shell water molecules (as shown in Table 1) are presented. The following six models, which span an important range of underlying interactions, are examined in the Results section:

Table 1. Parameters for the Models Analyzed in the Paper[a]

model	λ_h	λ_b	ε_{mm}	ε_{wm}	$\varepsilon\varepsilon_{hb}^{+}$	ε_g
I	1	0	0	0	0	0
II	1	0	0	0	−0.2	0
III	1	0	0	−0.3	0	0
IV	1	0	0	−0.6	0	0
V	0	0	−0.6	0	0	0
VI	0	0	−4.5	0	0	0
VII	1	0	0	0	−0.2	3.0
VIII	1	0	0	0	−0.2	2.0
IX	1	0	0	0	−0.2	1.0

[a] λ_h: hydration shell hydrogen bond tolerance; λ_b: bulk hydrogen bond tolerance, ε_{mm}(kcal/mol): interaction energy between nearest-neighbor monomers; ε_{wm}(kcal/mol): interaction energy between water and monomer nearest-neighbors; ε_{hb}^{+}(kcal/mol): enthalpy bonus for the hydration shell hydrogen bonds; ε_g: energetic preference of trans conformers over gauche.

- I: This model explores the effect of modeling the entropy penalty due to the reduced orientational freedom of water molecules around hydrophobic residues. This model has no interactions involving the homopolymer other than excluded volume.
- II: In addition to the orientational restriction of hydration shell water molecules of model I, there is an associated enthalpy bonus (ε_{hb}^{+} = −0.2 kcal/mol) for interfacial hydrogen bonds. The value of ε_{hb}^{+} is chosen to reproduce a result of atomistic simulation. This value yields the same hydrogen bond enthalpic gain of hydrophobic hydration shell water molecules when the homopolymer is collapsed as the one observed in a simulation of a β-hairpin in explicit water at physiological conditions (−0.32 kcal/mol).[38]
- III and IV: These models explore the effect of including attractive interactions (ε_{wm}) between water molecules and monomers on the collapse of the hydrophobic polymer. ε_{wm} of model IV is twice the one of model III and, at ambient temperature, is equal to kT.
- V and VI: These models examine the effect of including an intramolecular monomer interaction (ε_{mm}) for the homopolymer, in addition to the excluded volume effects. ε_{mm} of model V is equal to kT, whereas ε_{mm} of model VI has an order of magnitude greater strengh, similar to a water−water hydrogen bond.

By proper incorporation of effects such as local stiffness (ε_g) to model II, the hydrophobic polymer can be folded into a β-hairpin in the absence of any a priori preference for the formation of bends and site-specific interactions. To show the potential of the explicit water homopolymer model to explore protein folding and stability, the following three models are examined in the Results section (Table 1 summarizes the parameters):

- VII−IX: These sets of models explore the effect of adding a preference (ε_g) for t over g states (g^+ and g^-) to model II. By increasing the local stiffness ($\varepsilon_g^{VII} > \varepsilon_g^{VIII} > \varepsilon_g^{IX}$), we can investigate the effect of ε_g on the formation of a β-hairpin.

We note that in the current model, the number of hydrogen bonds formed in the liquid at a fixed temperature is controlled by q (results not shown). Thus, the temperature scale of the model is defined by the parameter q. The phase diagram of the

dx.doi.org/10.1021/jp3039175 | J. Phys. Chem. B 2012, 116, 8095−8104

pure liquid exhibits a vapor−liquid and a liquid−liquid equilibrium (results not shown) in agreement with previous work.[42,43] For $q \geq 840$, the solvent exhibits a vapor−liquid critical temperature in the range of [620 K, 660 K], in agreement with the experimental value of 647 K. The solvent also exhibits a liquid−liquid critical point in the range of [210 K, 260 K].

The fractional water density ρ_f of the system is selected so as to obtain a similar nn distribution of water molecules around a hydrogen-bonded pair as in an all-atom simulation of liquid water at physiological conditions.[38] The best agreement in the average number of nearest neighbors is obtained with $\rho_f = 0.66$, as shown in Figure 3. The average total nn binding energy of

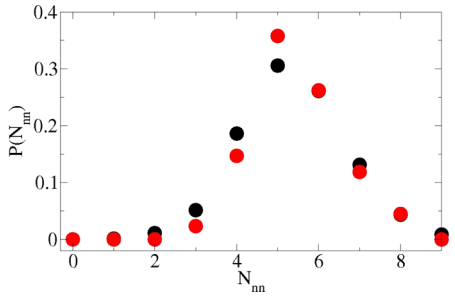

Figure 3. Comparison of the probability distribution for the number of nearest neighbors around a hydrogen-bonded water pair from a simulation of bulk water at physiological conditions[38] (black symbols) and from a simulation of bulk water using the lattice model described above (red symbols) with $\rho_f = 0.66$, $q = 840$, and $T = 300$ K.

water molecules is −16 kcal/mol for the lattice model at $\rho_f = 0.66$ and $T = 300$ K, whereas the one obtained from all-atom simulations of bulk water at ambient conditions is −14.5 kcal/mol.[38]

METHODS

Flat-histogram Monte Carlo (MC) methods are a growing class of techniques designed to enhance configurational sampling of complex systems.[44] These methods facilitate equilibration of complex systems by enhanced sampling of the energy space; the system is given a greater probability of escaping low-lying energy minima as compared to traditional Boltzmann sampling at low temperatures. In particular, we use the Wang−Landau algorithm[44] that directly yields information on the density of states (Ω) and consequently allows for the calculation of the system's properties as a function of temperature from one simulation. In the Wang−Landau method, the simulation performs a random walk in energy (E) with probability proportional to the reciprocal of the density of states, $1/\Omega(E)$ while recording the number of configurations visited for a given energy value $H(E)$. The random walk is performed within the range of attainable energies in the model. Trial moves from an old configuration (o) to a new one (n) at energies E_o and E_n, respectively, are accepted with probability

$$P_{acc}(o \rightarrow n) = \min\left[1, \frac{\Omega(E_o)}{\Omega(E_n)}\right] \quad (4)$$

Starting with an arbitrary choice of $\Omega = 1$ for all energy levels and $H(E) = 0$, the density of states is updated by multiplying the current value by a modification factor (f) each time a state with energy E is visited in the simulation, that is, $\Omega(E) \rightarrow \Omega(E)f$. At the beginning of the simulation, the modification factor is $f = f_{old} = e^1$ to allow the system to sample all possible energy levels efficiently. Whenever the monitored histogram of visits $H(E)$ is sufficiently flat, the modification factor is reduced to $f = (f_{old})^{1/2}$, and the histogram of visits is reset to 0. The process continues until the histogram is again sufficiently flat and the modification factor is reduced accordingly. This procedure is repeated until f approaches unity to within some tolerance. Here, our tolerance is chosen so that the simulation ends when the modification factor is less than $e^{10^{-6}}$.

Due to the large range of possible energy values that the system can explore (~2500 kcal/mol for the present model), the density of states is subdivided into 16 smaller overlapping regions for expediency. Adjacent subintervals have an overlap equal to half of their width. In the course of the simulation, we use configurations in the overlap region between energy intervals as starting configurations for the Wang−Landau simulation in lower-energy regions, thus ensuring that the different energy windows are also configurationally connected, as done previously by Rampf et al.[45] In a parallel implementation where each window runs independently, the computationally optimal distribution of energy windows occurs when the statistical error in the calculated results decreases at the same rate in each window. In this manner, each processor finishes the simulation at roughly the same time.[46] This motivates the choice of the size of each window.

The densities of states Ω in each window are merged together by minimizing the error in the overlap region between adjacent subintervals. The total error is defined as

$$e_{tot} = \sum_{i=1}^{N} \sum_{j=i+1}^{N} \sum_{k} [\ln \Omega_i(k) + C_i - \ln \Omega_j(k) - C_j]^2 \quad (5)$$

where N is the number of subintervals, k is an index for all overlapping bins of windows i and j, and the constants C are the values by which we can shift the density of states in each subinterval. In minimizing e_{tot} with respect to the constants C, we obtain N equations. By setting C_1 to 0, we solve the remaining $N - 1$ equations. Once all of the C constants are known, the final density of states is then pieced together from each shifted subsection; values of the overlap are averaged.

For the Wang−Landau simulation of the protein aqueous solution presented in the following section (the Results section), we use, for computational economy in this study, the value of $q = 168$, instead of the very large $q = 840$, which would give the physical temperature scale, and a polymer length of 14-mer. Nevertheless, the complete simulation sampling of the whole energy range of the aqueous solution 14-mer model with $q = 168$ required nearly 22000 CPU hours. The temperature (T) scale of the results presented in the Results section is in $\varepsilon_{hb}(6)/k$, where $\varepsilon_{hb}(6)$ is the hydrogen bond energy when there are six nearest neighbors around a hydrogen bond and k is the Boltzmann constant.

In order to extract more useful metrics of the system properties from the simulation data, the final results for the density of states are used in a subsequent simulation to measure the average properties of interest in each energy bin. Then, by reweighting the density of states to represent the canonical ensemble, the temperature dependence of average quantities of interest ($A(T)$) can be computed as follows

$$\langle A(T) \rangle = \frac{1}{Z(T)} \sum_{E} \Omega(E)\overline{A(E)}e^{-E/kT} \quad (6)$$

dx.doi.org/10.1021/jp3039175 | J. Phys. Chem. B 2012, 116, 8095−8104

where $Z(T)$ is the canonical partition function, $\Omega(E)$ is the density of states for energy E, and $\overline{A(E)}$ is equal to

$$\overline{A(E)} = \frac{1}{\Omega(E)} \sum_{x_E} A(x_E) = \frac{1}{H(E)} \sum_{x_E=1}^{H(E)} A(x_E) \quad (7)$$

where $H(E)$ is the number of visits to energy E and x_E runs over configurations at fixed energy.

RESULTS AND DISCUSSION

We present in this section the results obtained from a Wang–Landau simulation of a 14-mer homopolymer in explicit water for different parametrizations. First, we examine the effects on collapse transitions of the entropy penalty due to the increased orientational restrictions for water molecules around hydrophobic residues. Second, we quantify the effects of polymer–water attractions as well as monomer–monomer attractions. Third, we investigate the outcome of adding an enthalpic benefit for forming interfacial hydrogen bonds. Finally, we characterize the effect of adding local chain stiffness to the model in order to illustrate the potential of the explicit water–protein model to explore protein folding and stability.

Flexible Homopolymer. To investigate the influence of temperature on the spatial extent of the homopolymer, we characterize the temperature dependence of the average radius of gyration (R_g) for the six flexible homopolymer models as shown in Figure 4. Model I (blue curve), which has only

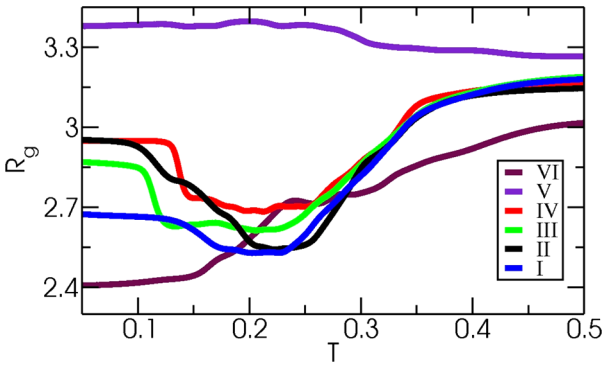

Figure 4. Temperature (T) dependence of the homopolymer radius of gyration (R_g, in units of the lattice constant). Each curve corresponds to a different model parametrization (see the text and Table 1; q = 168).

excluded volume interactions involving the homopolymer but does take into account orientational restrictions on interfacial water molecules, exhibits compact conformations when the temperature of the system is lowered from high temperatures. However, a further decrease in temperature results in a completely different scenario. As the temperature is decreased further from the region where the homopolymer is collapsed, a very mild swelling occurs. Cold-induced swelling is further enhanced by including an attractive water–monomer interaction (models III and IV), as shown by the green and red curves in Figure 4. The value of R_g in the collapsed region increases as ε_{wm} becomes more attractive, as can be seen by the destabilization of the collapsed state, in agreement with the previous work of Athawale and co-workers[24] using a traditional lattice-free all-atom water model to describe the solvent. In fact, for $|\varepsilon_{wm}| > 1.5$, the homopolymer cannot fold to a collapsed state anymore (results not shown).

Without the entropic penalty for interfacial water molecules, and if the monomer–monomer attraction is weak (model V), the homopolymer does not show a collapsed region, as shown by the violet curve in Figure 4. Otherwise, if there is a strong monomer–monomer attraction, the homopolymer folds into a collapsed state, as shown by the indigo curve (model VI). However, cold denaturation is not observed in the latter case. This result suggests that in order to observe cold-induced denaturation, the homopolymer collapse must be driven by an entropy effect involving the interfacial water molecules rather than an enthalpy effect within the polymer chain. Therefore, minimalist models of proteins that renormalize the role of water into effective interactions do not capture any of the physics of cold denaturation because the collapse transition in those models occurs in essence via an enthalpy effect within the polymer chain.

As shown in Figure 4 by the black curve (model II), the effect of adding an extra enthalpic benefit ($\varepsilon_{hb}^{+} < 0$) for hydrogen bonds involving at least one interfacial water molecule is to destabilize partially folded structures at low temperatures without destabilizing the collapsed state. The small extra enthalpic benefit for forming interfacial hydrogen bonds favors unfolding only at low temperatures, apparently because as the temperature increases, there is a reduction in the number of hydrogen bonds. This behavior is different from that associated with increasing the water–monomer attraction, which triggers a less pronounced hydrophobic collapse. For the models that exhibit cold denaturation (I–IV), the cold-unfolded state has a lower R_g compared to the heat-unfolded one, consistent with experimental evidence.[4]

The folded state of the protein is evidently correlated with a reduction in the number of interfacial water molecules around the exposed monomers, as shown in Figure 5. It is particularly

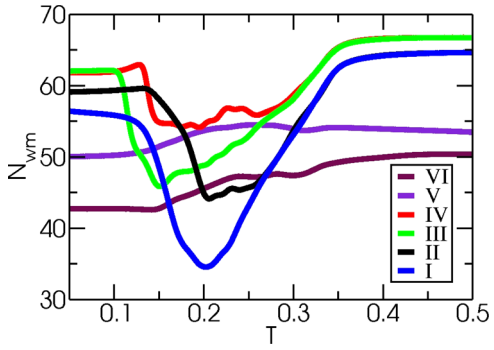

Figure 5. Temperature (T) dependence of the number of monomer–water contacts (N_{wm}). Each curve corresponds to a different model parametrization (see the text and Table 1; q = 168).

worth noting, although expected, that when either $\varepsilon_{hb}^{+} < 0$ (model II, black curve) or $\varepsilon_{wm} < 0$ (model III, green curve; IV, red curve), the number of water–monomer contacts in the collapsed state increases as ε_{hb}^{+} or ε_{wm} become favorable, as is clear when comparing to model I (blue curve) in which these energetic parameters are 0. The number of water–monomer interactions at high temperatures is not significantly affected by including an extra enthalpic benefit for forming interfacial hydrogen bonds; the black (model I) and blue (model II) curves coincide at high temperatures.

To further investigate the low-temperature homopolymer structure, we have computed the number of monomer–water–monomer contacts (water bridges, N_B). N_B is defined as the

dx.doi.org/10.1021/jp3039175 | J. Phys. Chem. B 2012, 116, 8095–8104

number of water-mediated contacts wherein a water molecule is a nearest neighbor to monomers i and $j \geq i + 3$. This definition of N_B quantifies the extent to which a homopolymer is solvent-penetrated, a signature of cold unfolding. The temperature dependence of N_B (Figure 6) shows that this quantity increases

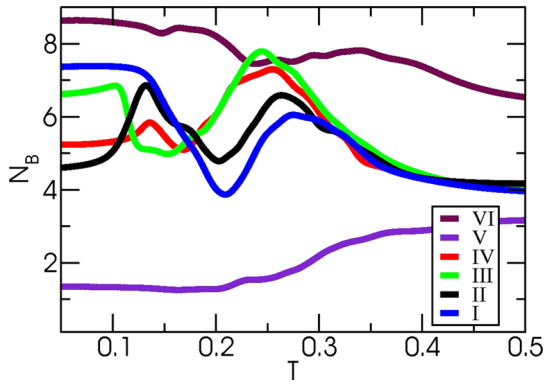

Figure 6. Temperature (T) dependence of the number of monomer–water–momer contacts (N_B). Each curve corresponds to a different model parametrization (see the text and Table 1; q = 168).

monotonically upon cooling at sufficiently low temperatures for model I (blue curve) because the cold-unfolded conformation for this model is compact (see Figure 4). An insertion of water molecules is observed for models II and IV (black and red curves) because N_B increases as the temperature is decreased away from the region where the homopolymer is collapsed. This trend continues until the number of water-mediated interactions achieves its maximum, when the homopolymer is wet and partially collapsed. If $\varepsilon_{hb} < 0$ (model II), the homopolymer continues to further unfold upon lowering the temperature with the number of water–monomer interactions constant (black curve in Figure 5), thus causing a reduction of water-mediated interactions. For the models that exhibit a stability window (models I–IV), decreasing the temperature from the heat-unfolded state causes an increase in N_B, indicating that while the homopolymer is collapsing, the partially collapsed structure is solvent-penetrated. Upon decreasing the temperature even further, N_B decreases, indicating an expulsion of water molecules from the hydrophobic core upon final folding. A different scenario is observed when the homopolymer collapse is driven by monomer–monomer attractions (model VI, indigo curve). In this case, N_B mildly increases monotonically as the temperature is lowered from the heat-unfolded state without an expulsion of water molecules upon hydrophobic collapse. In addition, it achieves almost a constant behavior at low temperatures.

A representative of a collapsed conformation is shown in Figure 7c. Upon increasing the temperature from the collapsed state, the homopolymer gradually unfolds and exposes more hydrophobic monomers to the solvent. The thermally denatured protein is an ensemble of conformations; illustrative structures are shown in Figure 7d,e. Although the heat-induced denaturation does lead to quantitatively more extended conformations (see Figure 4), it is evident from comparison of Figures 6a and 6b (cold-unfolded structures) to Figures 6d and 6e (thermally unfolded structures) that the qualitative differences are somewhat subtle. Both extremes lead to both partially unfolded and fully extended conformations. This contrasts with the structure from the cold-denatured state of the 2D water-explicit protein model that some of the present authors have previously developed;[31] there, the cold state is not an ensemble of disordered protein conformations; rather, it is a completely extended conformation for homopolymers and a single collapsed structure with a disrupted hydrophobic core for heteropolymers.[32]

To quantify the specific role of water in cold denaturation, the temperature dependence of the mean dimer energy (defined as the interaction energy between nn water molecules) of shell–shell and bulk–bulk water molecule pairs is shown in

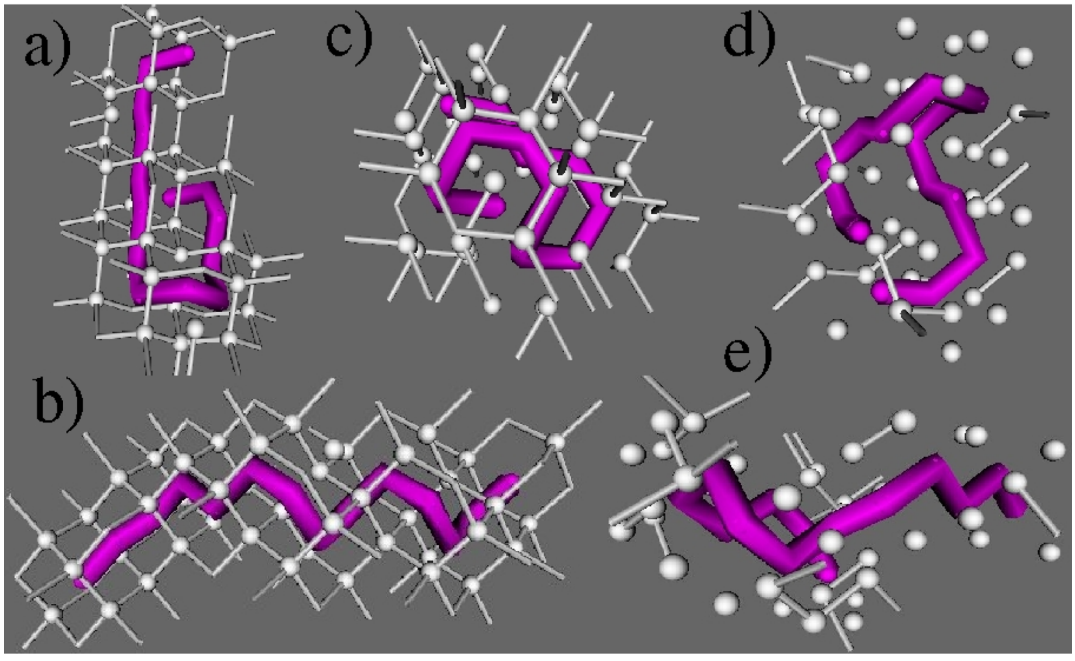

Figure 7. Representative conformations for a 14-mer model protein (model II) in the cold-unfolded state (a,b), native state (c), and thermally denatured state (d,e). Hydration water molecules are shown as white spheres, and hydrogen bonds are shown as line segments.

dx.doi.org/10.1021/jp3039175 | J. Phys. Chem. B 2012, 116, 8095–8104

Figure 8, where the dashed lines are for bulk pairs and the solid lines are for interactions within the hydration shell. Figure 8a

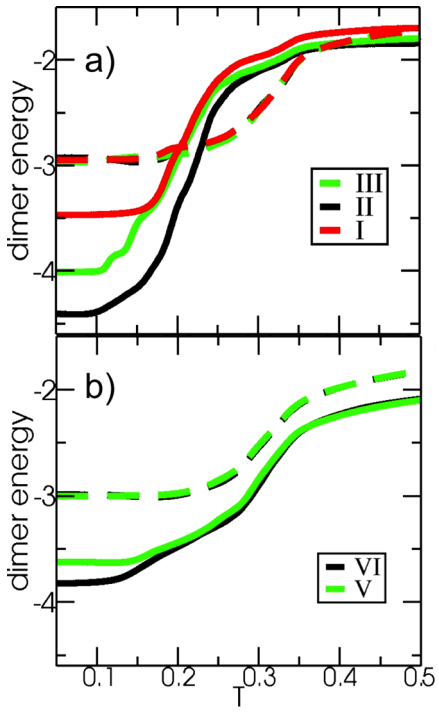

Figure 8. Temperature (T) dependence of the mean dimer energy (kcal/mol) for shell−shell and bulk−water interactions (see the text and Table 1; q = 168). Labels on the curves correspond to models defined in Table 1. The curves in (a) are for models that exhibit cold unfolding, and the ones in (b) correspond to models that do not exhibit cold unfolding. Dashed lines correspond to bulk−bulk dimer energies and continuous ones to shell−shell dimer energies.

provides the results for the models that exhibit both heat- and cold-induced denaturation, and Figure 8b provides results for the models that only exhibit heat denaturation. The dimer energy becomes more negative as the temperature is reduced in all cases. However, the temperature dependence for shell dimers is quite different from that of the bulk for the models, as shown in Figure 8a, where the formation of shell hydrogen bonds is more restrictive than that for bulk, and hence, an entropic penalty exists for forming hydration shell hydrogen bonds (λ_B = 1; λ_h = 0). In cases where cold denaturation takes place, as the temperature is lowered, the dimer energy for shell waters transitions from values that are less stable than those of the bulk to values more stable than those of the bulk, and this transition is distinctly more sensitive to temperature than that in the bulk. The sensitivity is consistent with the signature heat capacity increment that is typically associated with hydrophobic hydration.[2,47] The fact that the hydrogen-bonded structures are well-ordered around the hydrophobic groups is suggested by the heavily hydrogen-bonded hydration shells evident in the representative structures of the cold-unfolded state shown in Figures 7a and 7b. Therefore, cold denaturation occurs with an associated release of heat from the hydration shell, while in heat-induced denaturation, the hydration shell absorbs heat. This behavior is in agreement with experimental observations of heat and cold denaturation of proteins[2] and theoretical work by Dias and co-workers.[34] The fact that interfacial water molecules are stabilized at low temperatures is also suggested by the increase of water−monomer contacts at low temperatures after the hydrophobic collapse, as shown in Figure 5 for models I−IV.

If there is no entropic penalty for forming interfacial hydrogen bonds in the model, as is the case for those models that do not exhibit a stability window (Figure 8b), then the hydration shell hydrogen bond energies are seen to remain more stable than those in the bulk over the entire temperature range. Depending on the relative strength of intrapolymer attractive interactions, it is clear (see Figure 5) that the lack of an entropic penalty in the hydration shell can lead to either folding (model VI, indigo) or unfolding (model V, violet) upon lowering temperature, but it is also clear that the model fails to manifest a temperature window of collapsed states with both an upper and lower limit.

In summary, the homopolymer can be folded by either attractive interactions between the monomers (model VI) or by modeling the entropic cost of forming interfacial hydrogen bonds (models I−IV). However, cold denaturation is only observed when the enthalpic benefit of forming additional interfacial water molecules overcomes the enthalpic benefit of forming monomer−monomer interactions. Hence, cold denaturation is not observed if the homopolymer collapse is driven by intrapolymer attractions, rather than solvent enthalpy. The decreasing free-energy penalty on the occurrence of interfacial solvent with decreasing temperature, originating in the solvent orientational entropy contribution, leads to the formation of an additional polymer−solvent interface as the temperature is lowered, driving the homopolymer to cold unfold.

Formation of a β-Hairpin. To investigate the effects of including local chain stiffness in the protein model, and, in particular, the potential influence on homopolymer conformation, we compare below the results from models VII−IX, which differ in the degree of chain stiffness (see the Model Description section). We regard the inclusion of ε_g, the magnitude of a priori energetic preference for the trans over gauche conformation, as an addition to the basic parametrization of model II and investigate how the collapsed structures change depending on ε_g (Figure 9). Models VII−IX have decreasing preference for the trans state, with model VII having a strong preference of about $6kT$ and model IX have a modest preference of roughly $1.5kT$. Figure 10 shows representative structures of model VIII. The dependence of the radius of gyration on the value of ε_g is shown in Figure 9 by the red line (model VII), black line (model VIII), and green

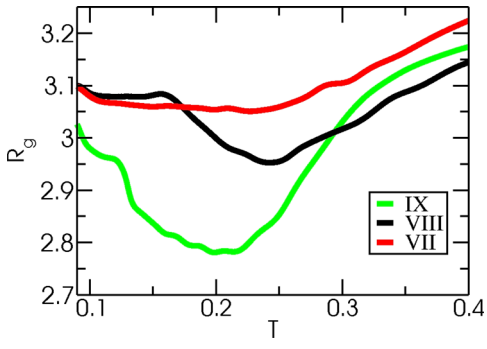

Figure 9. Temperature (T) dependence of the radius of gyration (R_g) of the homopolymer with chain stiffness. Each curve corresponds to a different model parametrization (see the text and Table 1; q = 168).

dx.doi.org/10.1021/jp3039175 | J. Phys. Chem. B 2012, 116, 8095−8104

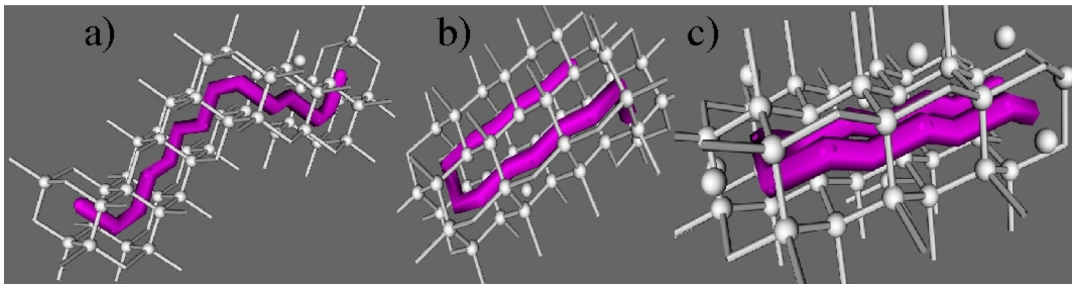

Figure 10. Representative conformations for a 14-mer model protein when local chain stiffness is incorporated by allowing a preference for trans over gauche states in the chain. For the model (model VIII), the cold-unfolded state (a) is relatively stiff compared to model II, as is evident from the completely extended conformation. The collapsed homopolymer is an ensemble comprised of a majority β-hairpin conformation where there are shifts in registry (b,c).

line (model IX). As is evident from Figure 9, depending on the degree of local stiffness, the homopolymer can exhibit polymer collapse over a limited temperature range. One finds that the collapsed structure can be dominated by a β-hairpin (model VIII) or exhibit a mixture of collapsed structures similar to the completely flexible homopolymer, with β-hairpin-like structures among them (model IX, green). If the degree of chain stiffness is quite large (ε_g = 3.0 kcal/mol, model VII), homopolymer collapse is greatly suppresed. The percentage of β-hairpin conformations in the ensemble of collapsed conformations depends nonmonotonically on the value of ε_g. For ε_g = 3.0 kcal/mol (model VII), the percentage of β-hairpin conformations in the relatively small population of collapsed conformations is 20%, for ε_g = 2.0 kcal/mol (model VIII), it is 70%, and for ε_g = 1.0 kcal/mol (model IX), it is 15%.

Due to the fact that the chain is a homopolymer, a perfect β-hairpin, as well as non-native states where there are shifts in registry due to differing locations of the bend, can been seen in the collapsed state of model VIII, as shown in Figure 10b,c. Figure 11 shows the temperature dependence of the fraction of

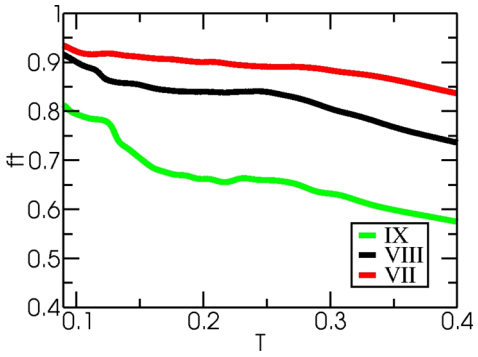

Figure 11. Temperature (T) dependence of the average fraction of trans states in the chain (ft) with chain stiffness; q = 168. Each curve corresponds to a different model parametrization (see the text and Table 1; q = 168).

trans states in the chain (ft). Not surprisingly, because the trans state is energetically favored in all three models, the fraction of trans states in the chain (ft) increases as the temperature decreases. Thus, for these three models, the cold-denatured state is stiffer than the heat-denatured state. It can be seen from the black curve (model VIII) that when the degree of chain stiffness is chosen to achieve a β-hairpin in the collapsed state, it leads to only relatively small reductions in protein size relative to the heat-unfolded state. In fact, a large fraction of trans state chain conformers are present in the heat-unfolded state. For the flexible homopolymer models I–VI, the cold- and heat-denatured state have ft = 0.3, whereas ft for the heat-denatured state of models VIII–IX is more than twice as large. Thus, the homopolymer is not a "coil" in the heat-denatured state for these models. Moreover, the cold-denatured state for models VII and VIII is a fully extended conformation, as shown in Figure 10a. This indicates that a more realistic model will need the introduction of intrinsically flexible "turn" residues.[27]

CONCLUDING REMARKS

We have developed from first principles a three-dimensional lattice model for an all-hydrophobic homopolymer in explicit water, based on the energetics of solvation of hydrophobic solutes simulated with all-atom models.[38] The protein structural representation[40,41] allows for the formation of secondary structural elements, and the water-explicit model presented here has been shown to exhibit both cold- and heat-induced unfolding for parameter choices that are consistent with our earlier atomistic simulation.[38] We have shown that the homopolymer can be folded by either including relatively large attractive interactions between the monomers or modeling orientational restrictions for water in the hydration shell, creating an entropic cost of forming hydrogen bonds in the vicinity of hydrophobic residues. However, the manifestation of a protein collapsed state that is stable only over a range bounded both at high and low temperature is only observed for the case when the homopolymer folding is driven by the entropic effect.

We have also found a mechanistic difference between cold and heat unfolding. The fact that hydrogen bonds involving interfacial water molecules are more favorable enthalpically than hydrogen bonds in bulk water is what drives cold unfolding at low temperatures in this model. Cold denaturation occurs with an associated release of heat from the hydration shell, whereas in heat-induced denaturation, the hydration shell absorbs heat.

We have also briefly explored the secondary structure for the homopolymer model. We have presented the case of a β-hairpin, but the protein model can adopt α-helix geometries,[40,41] and such structures will be the subject of further studies. In order to obtain a β-hairpin as the collapsed structure in the present model, the degree of chain stiffness is rather large. The homopolymer possesses a relatively high fraction of trans states in both cold- and heat-unfolded states. In addition, the possibility of forming a bend in different positions due to the fact that the chain is a homopolymer limits realism, and a

dx.doi.org/10.1021/jp3039175 | J. Phys. Chem. B 2012, 116, 8095–8104

model with at least hydrophobic, hydrophilic, and turn (flexible) residues[27] is desirable.

Our proposed model opens the door to validate phenomenological models such as the recent implicit solvent model by Dias and co-workers[48] that links motif propensities to effective interactions and desolvation barriers of residues. Future work focusing on exploring the role of hydrophobicity in secondary structural preferences is of considerable interest.

AUTHOR INFORMATION

Corresponding Author

*E-mail: matysiak@umd.edu.

Notes

The authors declare no competing financial interest.

ACKNOWLEDGMENTS

We are indebted to Dr. Lauren Kapcha for her insightful comments on an earlier version of this paper. P.G.D. and P.J.R. gratefully acknowledge the support of the National Science Foundation (Collaborative Research Grants CHE0404699 and CHE0908265 (P.G.D.) and CHE0404695 and CHE0910615 (P.J.R.)) and the R.A. Welch Foundation (F0019 (P.J.R.)). We are also grateful to the Texas Advance Computing Center (TACC) at the University of Texas for high-performance computing resources.

REFERENCES

(1) Hawley, S. A. *Biochemistry* **1971**, *10*, 2436−2442.
(2) Privalov, P. L. *Crit. Rev. Biochem. Mol. Biol.* **1990**, *25*, 281.
(3) Creighton, T. E., Ed. *Proteins: Structures and Molecular Properties*, 2nd ed.; W. H. Freeman: New York, 1993.
(4) Davidovic, M.; Mattea, C.; Qvist, J.; Halle, B. *J. Am. Chem. Soc.* **2008**, *131*, 1025−1036.
(5) Babu, C. R.; Hilser, V. J.; Wand, A. J. *Nat. Struct. Biol.* **2004**, *11*, 352−357.
(6) Jonas, J.; Ballard, L.; Nash, D. *Biophys. J.* **1998**, *75*, 445−452.
(7) Lopez, C. F.; Darst, R. K.; Rossky, P. J. *J. Phys. Chem. B* **2008**, *112*, 5961−5967.
(8) Sabelko, J.; Ervin, J.; Gruebele, M. *J. Phys. Chem. B* **1998**, *102*, 1806−1819.
(9) Hatley, R. H. M.; Franks, F. *FEBS Lett.* **1989**, *11*, 171−173.
(10) Adrover, M.; Esposito, V.; Martorell, G.; Pastore, A.; Temussi, P. A. *J. Am. Chem. Soc.* **2010**, *132*, 16240−16246.
(11) Adrover, M.; Martorell, G.; Martin, S. R.; Urosev, D.; Konarev, P. V.; Svergun, D. I.; Daura, X.; Temussi, P.; Pastore, A. *J. Mol. Biol.* **2011**, *417*, 413−424.
(12) Shan, B.; McClendon, S.; Rospigliosi, C.; Eliezer, D.; Raleighr, D. P. *J. Am. Chem. Soc.* **2010**, *132*, 4669−4677.
(13) Riccio, A.; Graziano, G. *Proteins: Struct. Funct. Genet.* **2011**, *79*, 1739−1746.
(14) Romero-Romero, M. L.; Ingles-Prieto, A.; Ibarra-Molero, B.; Sanchez-Ruiz, J. M. *PLos One* **2011**, *6*, e23050.
(15) Jayachandran, G.; Vishal, V.; Pande, V. S. *J. Chem. Phys.* **2006**, *124*, 164902.
(16) Day, R.; Paschek, D.; Garcia, A. E. *Proteins: Struct. Funct. Genet.* **2010**, *78*, 1889−1899.
(17) Zhou, R.; Berne, B. J.; Germain, R. *Proc. Natl. Acad. Sci. U.S.A.* **2001**, *98*, 14931−14936.
(18) Rhee, Y. M.; Sorin, E. J.; Jayachandran, G.; Pande, V. J. *Proc. Natl. Acad. Sci. U.S.A.* **2004**, *101*, 6456−6461.
(19) Shea, J.-E.; Onuchic, J. N.; Brooks, C. L. *Proc. Natl. Acad. Sci. U.S.A.* **2002**, *99*, 16064.
(20) Zhou, R.; Huang, X.; Margulis, C. J.; Berne, B. J. *Science* **2004**, *305*, 1605−1609.
(21) Paschek, D.; Nonn, S.; Geiger, A. *Phys. Chem. Chem. Phys.* **2005**, *7*, 2780−2786.
(22) Paschek, D.; Gnanakaran, S.; Garcia, A. E. *Proc. Natl. Acad. Sci. U.S.A.* **2005**, *102*, 6765−6770.
(23) Paschek, D.; Hempel, S.; Garcia, A. E. *Proc. Natl. Acad. Sci. U.S.A.* **2008**, *105*, 17754−17759.
(24) Athawale, M. V.; Goel, G.; Ghosh, T.; Truskett, T. M.; Garde, S. *Proc. Natl. Acad. Sci. U.S.A.* **2007**, *104*, 733−738.
(25) Matysiak, S.; Clementi, C. *J. Mol. Biol.* **2006**, *363*, 297−308.
(26) Hubner, I. A.; Oliveberg, M.; Shakhnovich, E. I. *Proc. Natl. Acad. Sci. U.S.A.* **2004**, *22*, 8354−8359.
(27) Honeycutt, J. D.; Thirumalai, D. *Biopolymers* **1992**, *32*, 695−709.
(28) Yap, E.; Fawzi, N. L.; Head-Gordon, T. *Proteins* **2008**, *70*, 626−638.
(29) Matysiak, S.; Clementi, C. *Arch. Biochem. Biophys.* **2008**, *469*, 29−33.
(30) Whitten, S. T.; Kurtz, A. J.; Pometum, M. S.; Wand, A. J.; Hilser, V. J. *Biochemistry* **2006**, *45*, 10163.
(31) Patel, B. A.; Debenedetti, P. G.; Stillinger, F. H.; Rossky, P. J. *Biophys. J.* **2007**, *93*, 4116−4127.
(32) Patel, B. A.; Debenedetti, P. G.; Stillinger, F. H.; Rossky, P. J. *J. Chem. Phys.* **2008**, *128*, 175102.
(33) Marques, M. I.; Borreguero, J. M.; Stanley, H. E.; Dokholyan, N. V. *Phys. Rev. Lett.* **2003**, *91*, 138103.
(34) Dias, C. L.; Ala-Nissila, T.; Karttunen, M.; Vattulainen, I.; Grant, M. *Phys. Rev. Lett.* **2008**, *100*, 118101.
(35) Caldarelli, G.; De Los Rios, P. *J. Biol. Phys.* **2001**, *27*, 229−241.
(36) Zichi, D. A.; Rossky, P. J. *J. Chem. Phys.* **1985**, *83*, 797−808.
(37) Rossky, P. J.; Zichi, D. A. *Faraday Symp. Chem. Soc.* **1982**, *17*, 69−78.
(38) Matysiak, S.; Debenedetti, P. G.; Rossky, P. J. *J. Phys. Chem. B* **2011**, *115*, 14859−14865.
(39) Sikorski, A.; Skolnick, J. *Proc. Natl. Acad. Sci. U.S.A.* **1989**, *86*, 2668−2672.
(40) Kolinski, A.; Skolnick, J.; Yaris, R. *Biopolymers* **1987**, *26*, 937−962.
(41) Sikorski, A.; Skolnick, J. *Proc. Natl. Acad. Sci. U.S.A.* **1989**, *86*, 2668−2672.
(42) Roberts, C. J.; Debenedetti, P. G. *J. Chem. Phys.* **1996**, *105*, 658−672.
(43) Roberts, C. J.; Karayiannakis, G. A.; Debenedetti, P. G. *Ind. Eng. Chem. Res.* **1998**, *37*, 3012−3020.
(44) Wang, F.; Landau, D. P. *Phys. Rev. E* **2001**, *64*, 056101.
(45) Rampf, F.; Binder, K.; Paul, W. *J. Polym. Sci., Part B: Polym. Phys.* **2006**, *44*, 2542.
(46) Shell, M. S.; Debenedetti, P. G.; Panagiotopoulos, A. Z. *J. Phys. Chem. B* **2004**, *108*, 19748−19755.
(47) Edsall, J. T. *J. Am. Chem. Soc.* **1935**, *57*, 1506−1507.
(48) Dias, C. L.; Karttunen, M.; Chan, H. S. *Phys. Rev. E* **2011**, *84*, 041931.